



LAWRENCE
LIVERMORE
NATIONAL
LABORATORY

Geomagnetic EMP Sources Radiating through a Gamma Shadow

H. W. Kruger

May 29, 2014

Journal of Radiation Effects, Research and Engineering

Disclaimer

This document was prepared as an account of work sponsored by an agency of the United States government. Neither the United States government nor Lawrence Livermore National Security, LLC, nor any of their employees makes any warranty, expressed or implied, or assumes any legal liability or responsibility for the accuracy, completeness, or usefulness of any information, apparatus, product, or process disclosed, or represents that its use would not infringe privately owned rights. Reference herein to any specific commercial product, process, or service by trade name, trademark, manufacturer, or otherwise does not necessarily constitute or imply its endorsement, recommendation, or favoring by the United States government or Lawrence Livermore National Security, LLC. The views and opinions of authors expressed herein do not necessarily state or reflect those of the United States government or Lawrence Livermore National Security, LLC, and shall not be used for advertising or product endorsement purposes.

Geomagnetic EMP Sources Radiating through a Gamma Shadow

Hans Kruger

Lawrence Livermore National Laboratory

Abstract

The author's 3D geomagnetic EMP code MACSYNC is used to investigate the sources of the EMP that radiate through the gamma shadow region produced by a lumped mass, located on the line-of-sight to the observer, for an urban terrorist nuclear attack scenario. Gamma attenuation by the mass reduces the ionization density and associated air conductivity in the shadow, causing an increase in the EMP amplitude and rise time. The emphasis of the current computations is on the extent to which air conductivity created by scattered gammas, crossing over from the unshadowed region into the shadow, clamp this amplitude increase.

Introduction

The effects of computing geomagnetic EMP in three dimensions, instead of the one-dimensional treatment used in legacy codes such as CHAP and HEMP, on rise time and shape of the electromagnetic pulse was discussed by the author in a recent JRERE paper for an isotropic gamma source.¹ The current paper will report results of additional computations with the author's 3D geomagnetic EMP code MACSYNC, exploring the effects of a three-dimensional gamma source distribution, produced when a lumped massive object is located on the line-of-sight (LOS) to the observer.

MACSYNC uses the MCNP Monte Carlo code, developed by the Los Alamos National Laboratory, for coupled gamma-electron transport and the author's subroutines to generate synchrotron radiation mini-pulses at each electron transport step.² Each of these electromagnetic mini-pulses is then attenuated on the way to the observer, using the author's space and time dependent radiation-induced air conductivity models, and vectorally added to yield the observed composite EM pulse.

Related MACSYNC computations, for an urban burst scenario with a long block of city buildings located across the LOS, have been reported by the author in another recent JRERE issue.³ The MACSYNC zoning for the current lumped-mass scenario was specifically set up to enable the investigation of conductivity effects within the shadow cone which was not possible with the zoning used for the city building block scenario.

Gamma shadow geometry

Masses that cast a gamma shadow in the direction of the observer are unavoidable for a ground or near-surface burst since local scenario features, such as buildings, storage tanks, automobiles, or other massive objects will attenuate the gammas. For the current computations, an idealized urban terrorist attack scenario with a nuclear device was chosen (see Figure 1). If this city were to be monitored with ground-based EMP sensors, some of these sensors could be expected to lie within a gamma shadow.

MACSYNC computations

In MACSYNC, the problem was set up as a point source in sea level air with a one meter thick metal plate located on the LOS subtending a half-angle of 20 degrees (see Figure 2). The density of the plate was varied for different computations to provide gamma attenuation factors of 0.4, 0.1, and values between $1e-2$ and $1e-8$ in steps of one decade. The calculations used a 3 Mev gamma source with a 0.01 shake (0.1 nanosecond) wide pedestal output pulse and a 0.5 gauss magnetic field perpendicular to the LOS. This pedestal pulse was chosen instead of a delta function as a convenient diagnostic tool that allowed a monitoring of the air conductivity build-up during the computation. The total yields were 1, 10, and 100 kt with a 0.3% gamma yield fraction.

The EMP radiating through the gamma shadow cone is generated by three sources, as sketched in Figure 2. One source consists of Compton electrons created in the unshadowed region sufficiently close to the cone surface for their EMP to reach and enter the shadow cone with little EM attenuation. The second source is made of Compton electrons created in the unshadowed region so close to the cone surface that they can cross over into the shadow and continue radiating there. The third source is due to Compton electrons created within the gamma shadow, either by scattered gammas that crossed over from the unshadowed region, or by gammas transmitted through the shadowing object.

The problem was set up with 100 meter wide spherical shell zones centered on the burst point. A 20 degree half-angle cone, with its apex at the source and centered on the LOS to the observer, cut through these spherical shells. This provided a separate set of spherical shell segment zones for the unshadowed and the shadowed regions.

MACSYNC operated with two sets of air conductivity models that were a function of the radius from the source and the time since first unscattered gamma arrival at that radius. One set was for the unshadowed region assuming a spherical point source. The other was for the shadowed region assuming zero gamma transmission through the shadowing object so that only scattered gammas, crossing over from the unshadowed region, can create ionization and conductivity in the shadow cone. Both these conductivity models were obtained from separate MCNP calculations using very high space and time resolution. Both models included conduction electron attachment between the time of ionization creation at a given radius and the time of arrival of the EM pulse at that radius. This feature is important for off-LOS propagation paths

where this time difference can allow significant reduction of conductivity due to electron attachment.

The conductivity versus time since first gamma arrival, for these two models, is plotted for radii of 500 and 1500 meters in Figures 3a and 3b. It can be seen from these Figures, that the conductivity due to cross-over scattered gammas becomes significant, compared to conductivity from 100% transmitted gammas, only at late times. However, when a shadowing object greatly reduces the transmitted gamma fraction, and with it the associated conductivity, the conductivity due to cross-over scattered gammas dominates. As a consequence, the conductivity is clamped at the value given by the cross-over scattered gammas and unaffected by further reductions in gamma transmission. (The discontinuities, apparent in the conductivity curves plotted in Figure 3, are artifacts of the routines used to fit the MCNP computations of space- and time-varying ionization density with mathematical expressions suitable for EMP computations. They occur at the smallest and largest radii covered by the fit, where the exact value of the conductivity does not matter since the air at these radii is either EMP-opaque or EMP-transparent.)

EMP-opaque volume around burst point

EMP transmission from a radiating electron, located a given radius from the burst point, to a distant observer can be calculated directly from these air conductivity models, without involvement of MACSYNC. Figure 4a shows such calculations for the transmitted-gamma conductivity model, while Figure 4b shows results for the cross-over scattered gamma conductivity model. Figure 4a contains two sets of curves. The dashed curves are for zero EMP arrival delay, i.e. immediately after ionization creation, for a range of gamma attenuations. The solid curves are for 100% gamma transmission and a range of EMP arrival times, following first gamma arrival. This delay between gamma and EMP arrival is the time available for conduction electron attachment. The curves in Figure 4b are for various EMP arrival times relative to speed-of-light traversal from the burst point, with the color code the same as for the solid lines in Figure 4a. The total yield in both Figures is 1 kt.

As can be seen from the solid curves in Figure 4a, the unshadowed region (100% gamma transmission) is initially completely opaque to EMP within ~1 km from the burst point for a total yield of 1 kt. It is 50% transparent at ~1.4 km and completely transparent beyond ~2 km. As the EMP arrival time increases, electron attachment increases the air EMP transmission and reduces the opaque volume.

In the gamma shadow, when the gamma transmission is very small so that the conductivity is determined by cross-over scattered gammas, the initial 50%-transparent radius is only ~550 m as shown in Figure 4b. For later arriving EMP, this radius increases to as much as ~800 m at 1 shake, because the continuing scattered gamma flux increases the conduction electron density more than electron attachment reduces it. Finally, after tens of shakes, the electron attachment

dominates and the 50%-transparent radius shrinks. It is back at ~550 m at ~100 shakes and reaches ~400 m at 1000 shakes.

Thus, one expected effect of a gamma shadow on the EMP shape is an increase in amplitude because of the reduced attenuation for EMP traveling through the shadow cone compared to EMP traversing the unshadowed region. A second expected effect is a reduction in the early-arriving part of the pulse, and an associated increase in pulse rise time, because the gamma attenuation decreases the number of Compton electrons generated near the LOS. It is this source region that has the shortest combined flight path for the gammas and their EMP and thus produces the leading part of the pulse.

Computed EM pulse shapes

As reported in Reference 1, 3D effects have a significant impact on EM pulse shapes, even in the absence of a gamma shadow. This is evident in Figure 5 which compares a 3D MACSYNC calculation for a 1kt ground burst with a corresponding calculation with the widely used 1D spherical HEMPV legacy code, using the same 0.01 shake (0.1 nanosecond) wide output pulse of 3 Mev gammas chosen for the other calculations in this paper.⁴ The detailed Monte Carlo treatment of Compton electron multiple scattering in MACSYNC, as opposed to HEMPV's obliquity factor approximation, is responsible for the ~2 nanosecond lower rise time bound on the leading edge of the MACSYNC pulse. The rise of the pulse at late times in the MACSYNC computation is caused by a combination of detailed Monte Carlo tracking of multiply scattered gammas, off-LOS EMP propagation, and reduced attenuation, due conduction electron attachment, for EMP arriving with a delay relative to first gamma arrival. HEMPV does not follow scattered gammas and cannot treat off-LOS EMP propagation since it is a one-dimensional code.

The introduction of a gamma shadow, in the MACSYNC computations, leads to a further increase of both the leading edge rise time and the peak amplitude of the EMP. This can be seen in Figure 6 which compares calculations with and without a gamma shadow. The shadowed calculations were done for the two models of air conductivity described in a preceding paragraph. For the transmitted-gammas conductivity model, calculations were done for gamma transmission values ranging from 0.4 to 1e-8. It can be seen from this Figure that the peak field increases as the gamma transmission decreases, until the increase saturates at 1e-6 gamma transmission at a value that is about two orders-of-magnitude larger than the peak field without a gamma shadow. Simultaneously, the peak shifts to earlier times with decreasing gamma transmission. However, these results for very small gamma transmission values do not properly reflect the effect of cross-over scattered gammas on the conductivity in the shadow cone. When the calculation is done with the cross-over scattered conductivity model, the peak field increase over the unshadowed value is clamped at a factor of approximately five. As can be seen from Figure 6, the leading edge rise time is also increased by a similar factor compared to the unshadowed rise time.

These shadowed and unshadowed pulse shapes are again compared in Figure 7, this time on a linear vertical scale, using the cross-over scattered gamma conductivity model in the shadow. This Figure also breaks down the total field into components from Compton electrons radiating either inside or outside the shadow cone. It can be seen that, for the unshadowed scenario, electrons radiating inside and outside the shadow cone contribute about the same peak field amplitude, but the radiation from the sources outside the cone arrive much later than those from inside the cone. This is expected from the geometry and the associated combined gamma and EMP flight paths. The introduction of the gamma shadow produces a large increase in the field radiated outside the shadow cone, while there is little increase in the field from sources inside the cone.

Additional MACSYNC calculations for the shadowed scenario, in which the gammas were stopped after their first scatter, show that less than one percent of the electrons radiating in the shadow are created by previously unscattered gammas. These are either electrons crossing over from the unshadowed region or electrons created by transmitted gammas. Thus more than 99% of the electrons radiating in the shadow are created by previously scattered gammas.

Finally, Figure 8 compares the shadowed and unshadowed total EM pulse shapes for yields of 1, 10, and 100 kt, again using the cross-over scattered gamma conductivity model in the shadow. It can be seen that the shadowed peak field amplitude is always larger than the unshadowed one by a factor of approximately five. The rise times of the shadowed leading EMP edges are also larger by about the same factor of five than those of the unshadowed leading edges.

The unshadowed MACSYNC calculation in Figure 5 used a full isotropic gamma source, while in the MACSYNC calculations shown in all the other Figures, the source was restricted to emitting gammas only over the hemisphere centered on the LOS and the results were normalized accordingly. This was done to improve the Monte Carlo statistics for the leading edge of the pulse. This restriction on the gamma emission angle had no effect at all on the positive part of the pulse. However, the late, negative part of the pulse, which was of no interest in this investigation, was affected. Its amplitude was reduced significantly.

The air conductivity in the shadowed region and its effect on the EM pulse will depend on the geometry of the shadow generated in a specific scenario. For example, for the scenario with a long city block obscuring the LOS to the observer, mentioned previously, the ionization density and associated air conductivity should be an order of magnitude lower than for the lumped mass scenario of this paper. The reason for this is that the scattered gammas do not surround the shadow and are at a larger average distance. As a consequence, the field increase due to the gamma shadow can be expected to be clamped at a higher value than for the lumped mass scenario of this paper.

Conclusions and Observations

The 3D computations discussed in this paper lead the author to the following conclusions:

1. Gamma shadows are unavoidable in real-world scenarios.
2. Gamma shadows can significantly increase both amplitude and rise time of geomagnetic EMP in ground and near-surface burst scenarios.
3. The magnitude of the amplitude increase is clamped by ionization in the shadow from scattered gammas crossing over from the unshadowed region. The extent of this clamping effect depends on the detailed geometry of the shadow generated in a specific burst scenario.

The author would like to offer these observations:

1. Since gamma shadow effects can impact EMP hardening standards and various National applications of EMP, it appears advisable to verify the predictions of MACSYNC with an EMP code using the more traditional method of computing the currents and solving Maxwell's equations on a spatial grid. This requires a 3D code with detailed coupled gamma-electron transport, very high spatial resolution, self-consistency, and air avalanche treatment. Such a code, which does not exist today, ought to be developed.
2. It also appears advisable to search EMP measurements from atmospheric nuclear tests for data relevant to gamma shadow effects, and to explore the feasibility of laboratory experiments with newly available radiation simulators that could help validate the computed gamma shadow effects on EMP.

Acknowledgement

The author thanks Dr. David Larson for his encouragement and support.

Prepared by LLNL under Contract DE-AC52-07NA27344

References

1. H. Kruger, "3D Effects in Geomagnetic EMP Computations", *Journal of Radiation Effects, Research and Engineering*, Vol. 31, No. 1, p. 159, July, 2013.
2. Los Alamos National Laboratory X-5 Monte Carlo Team, "MCNP – A General Monte Carlo N-Particle Transport Code, Version 5", LA-UR-03-1987, 20005.
3. H. Kruger, "Gamma Shadow Effects on Geomagnetic EMP Rise Time and Amplitude", *Journal of Radiation Effects, Research and Engineering*, Vol. 32, No. 1, p. 55, April, 2014.
4. W. E. Page et al, "A Description of the HEMP-B Computer Code", Air Force Weapons Laboratory Report AFWL-TR-73-286 (1975).

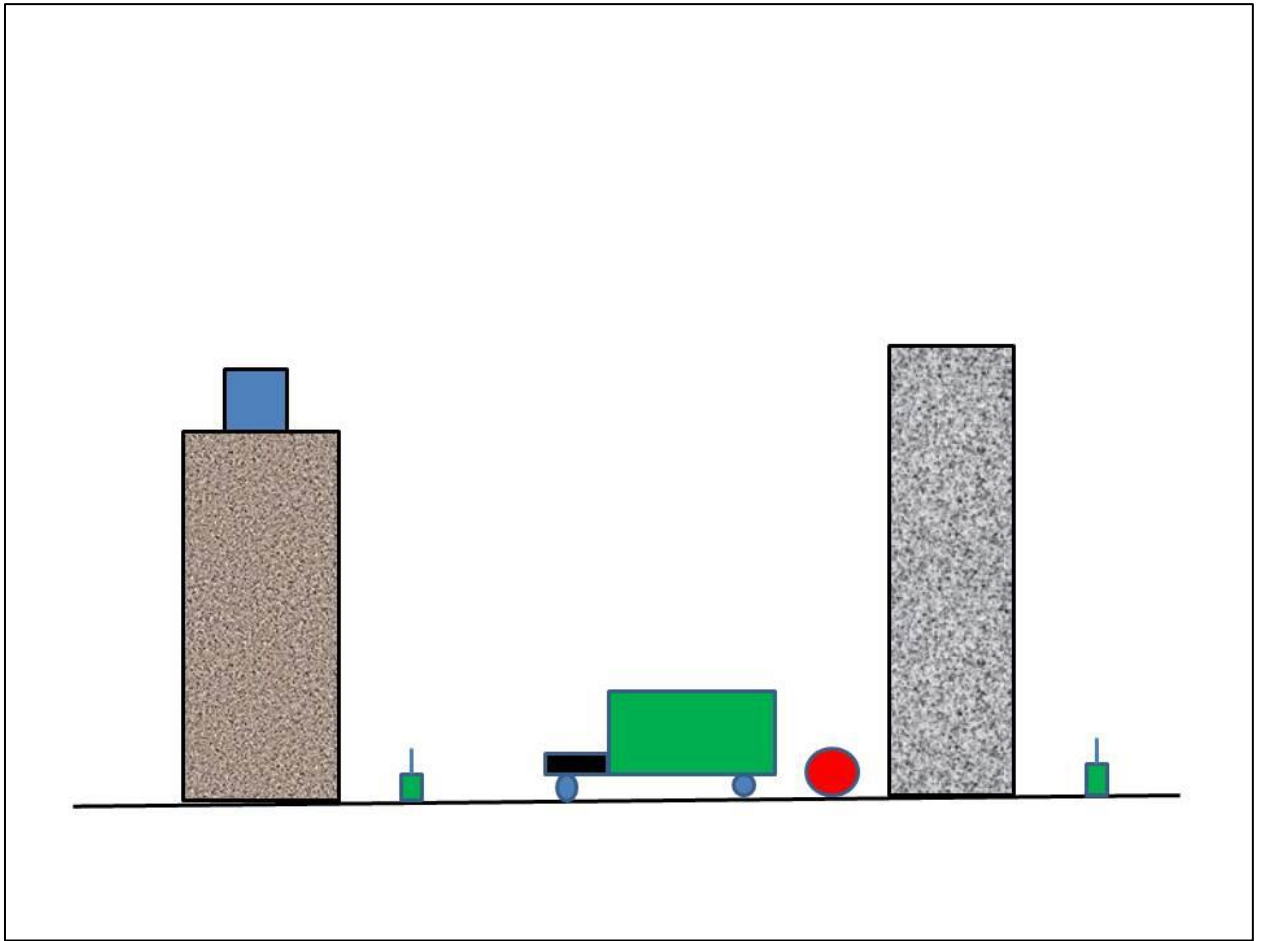


Figure 1.

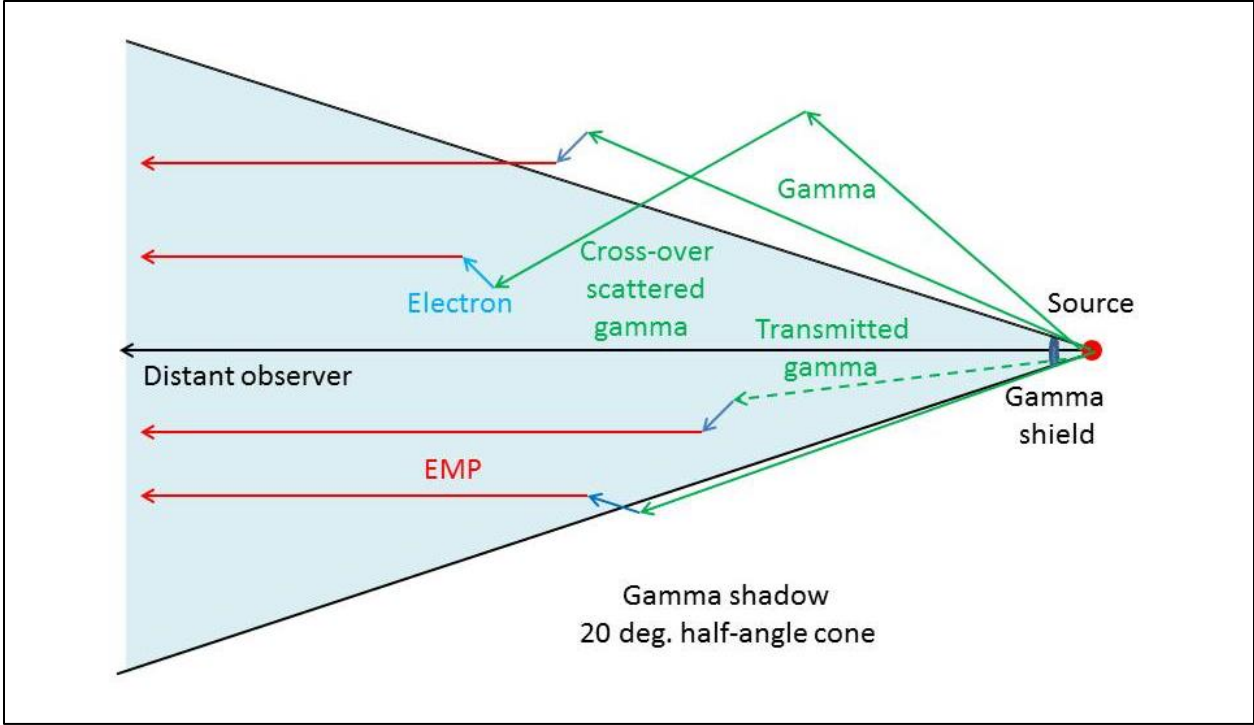


Figure 2.

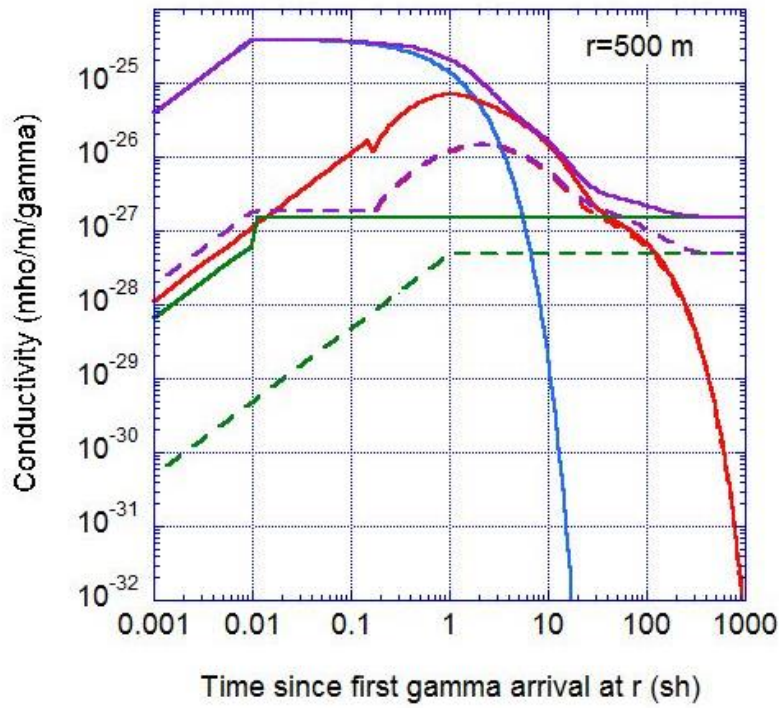


Figure 3a.

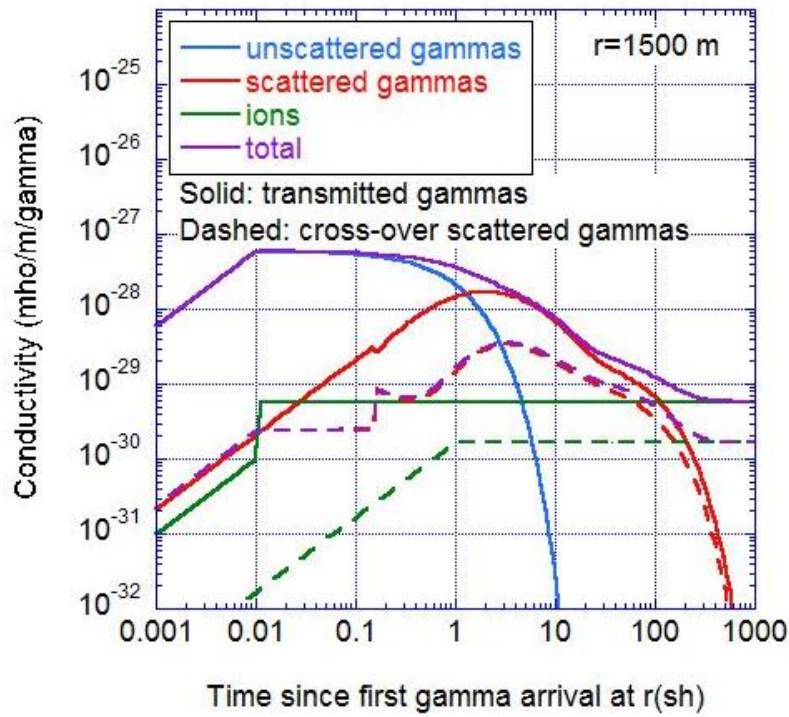


Figure 3b.

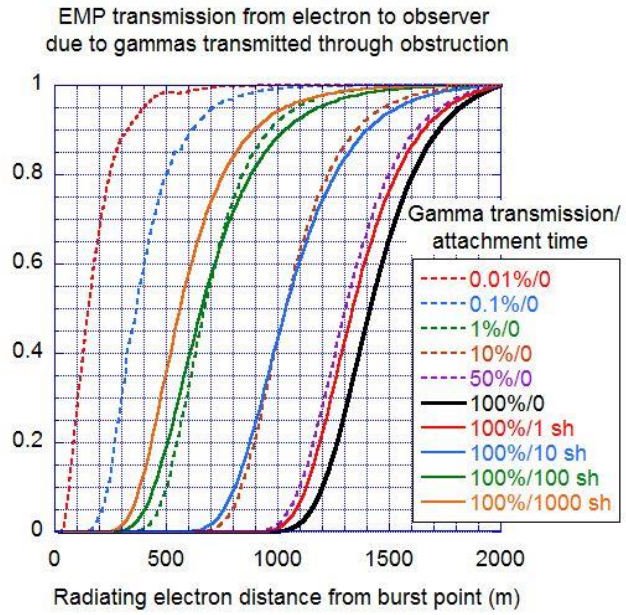


Figure 4a.

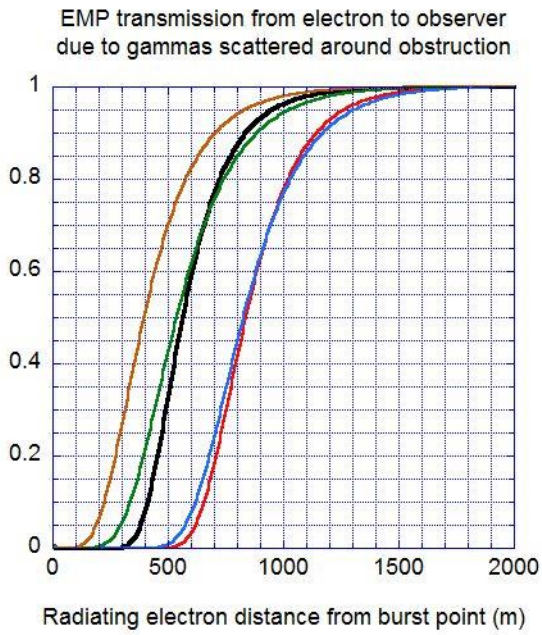


Figure 4b.

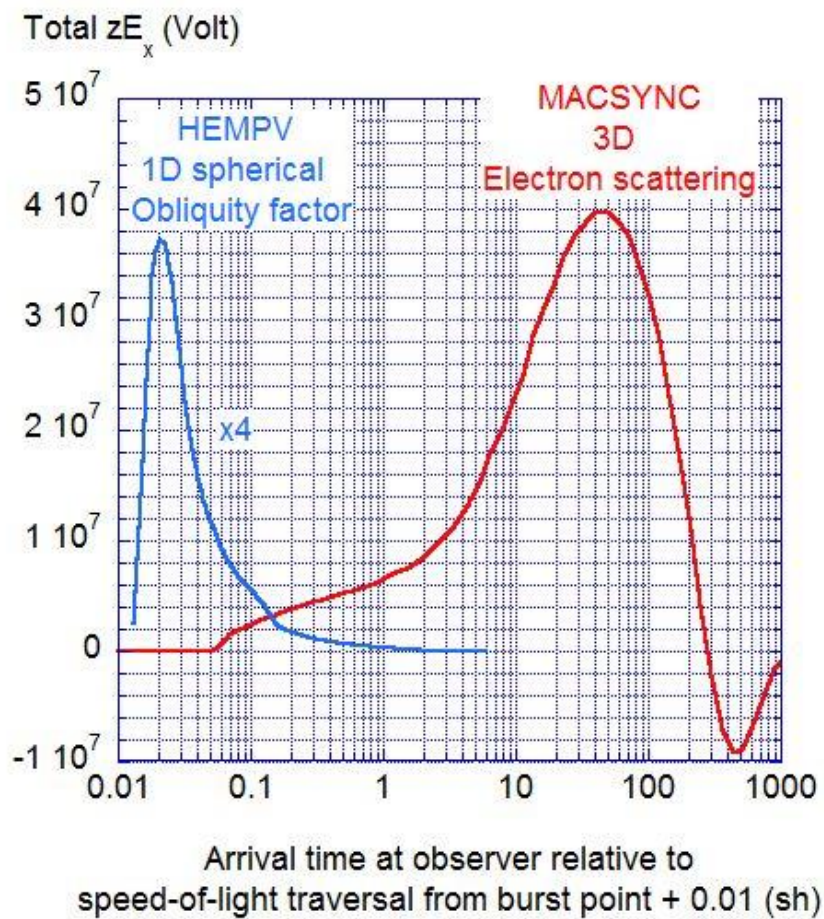


Fig. 5

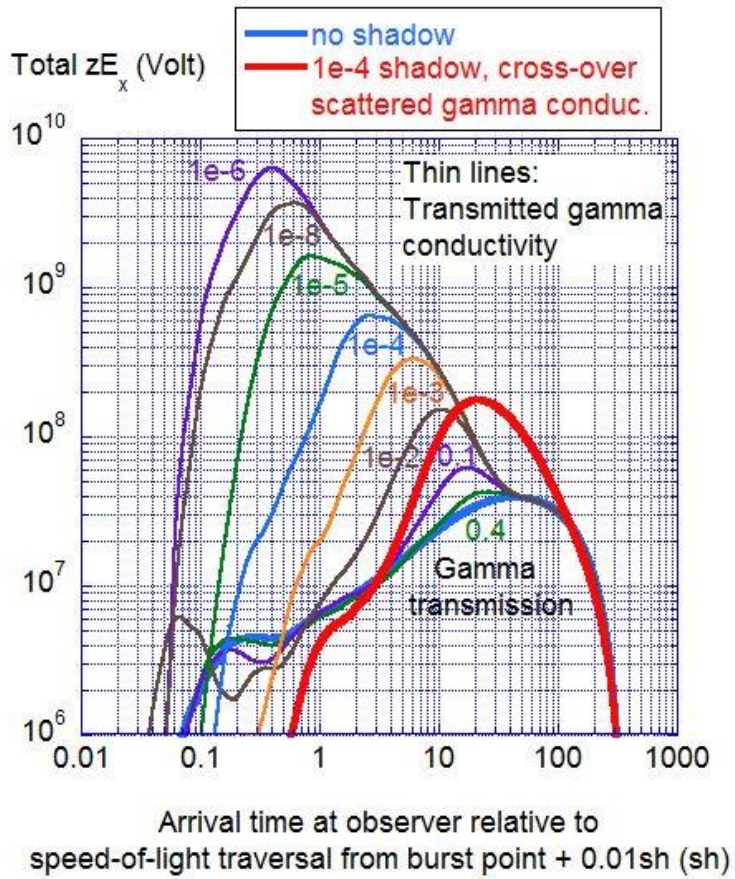


Fig. 6

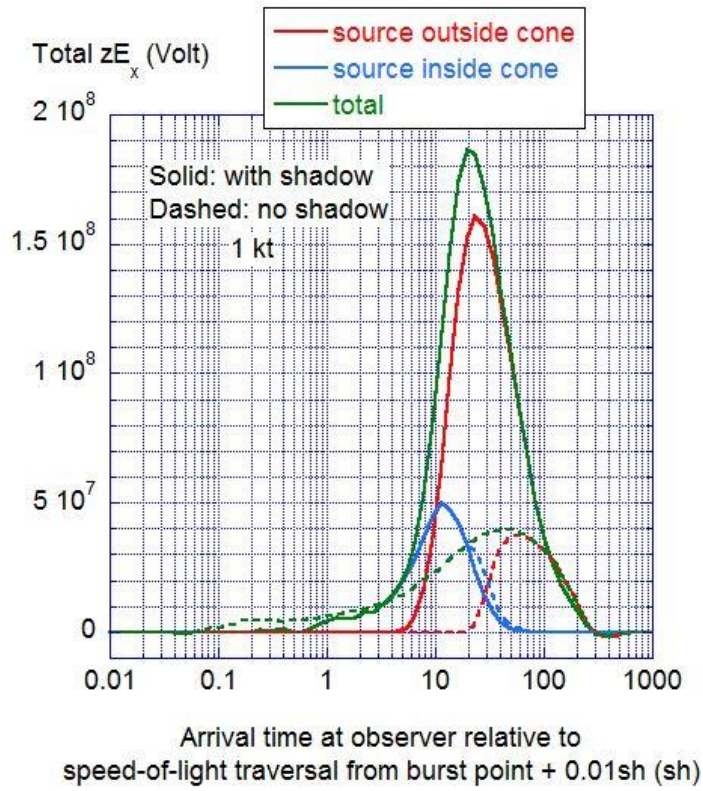


Fig. 7

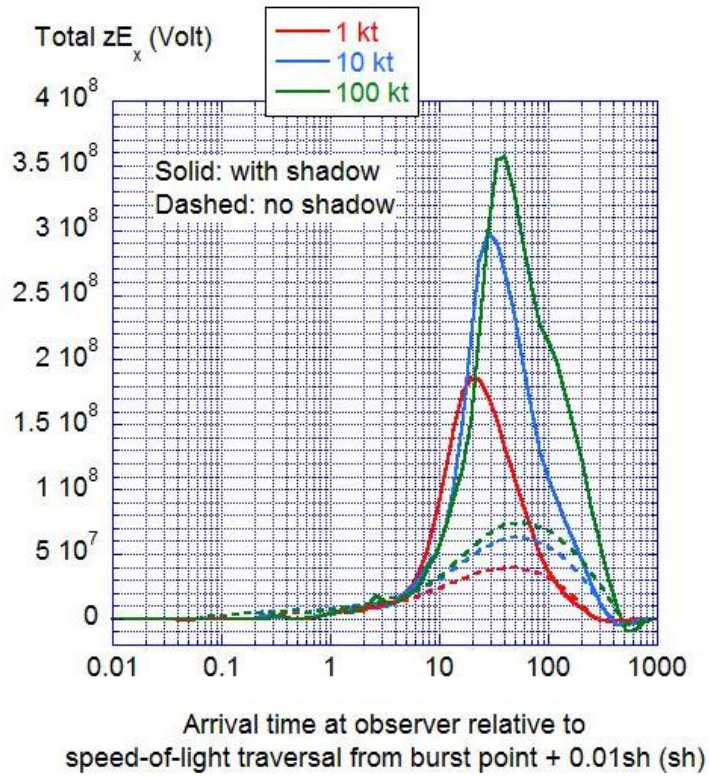


Fig. 8

Figure Captions

Fig. 1. Urban terrorist nuclear attack scenario with a nuclear device. Ground-based EMP sensors could lie in the gamma shadow cast by buildings, water tanks, automobile engines, or the many other massive objects present in urban settings.

Fig. 2. Geometry used in MACSYNC computations. A 1 meter thick gamma shield subtending a 20 degree half-angle is located on the line-of-sight to the observer. The density of the shield is varied to provide a wide range of gamma attenuation factors.

Fig. 3a. Radiation-induced air conductivity at a radius of 500 m from the burst. The solid lines are for gammas transmitted through the shield. As drawn, they are for 100% transmission. For lower transmission values, the conductivity scales with transmission. The dashed lines show the conductivity induced in the shadow for zero transmission through the gamma shield. This conductivity is principally caused by scattered gammas crossing over from the unshadowed region. The separate contributions to the total conductivity from unscattered or scattered gammas and from ions are shown. The total yield is 1 kt with a 0.3% gamma fraction. The energy of the gammas is 3 Mev. The pulse is a 0.1 nanosecond (0.01 shake) wide pedestal. This pedestal was chosen, instead of a delta function, since it provided a convenient diagnostic tool for monitoring the build-up of the air conductivity during the computation.

Fig. 3b. Radiation-induced conductivity at a radius of 1500 m. Comments of Fig.3a apply.

Fig. 4a. EMP transmission to a distant observer from an electron radiating at a distance r from the burst point, when ionization is caused by transmitted gammas. EMP transmission is shown for various values of gamma transmission and conduction electron attachment time, i.e. time between ionization creation at r and arrival of the EMP at that distance. Total yield 1 kt with a 0.3% gamma fraction. Gamma energy 3 Mev. Pulse width 0.1 nanosecond.

Fig. 4b. Same as Fig. 4a, but for ionization caused by gammas for zero gamma transmission, i.e. caused by scattered gammas crossing over from the unshielded region.

Fig. 5. Comparison of the EMP computed by MACSYNC and the widely used 1D spherical legacy code HEMPV for a total yield of 1kt with a 0.3% gamma fraction, a 3 Mev gamma energy, and a 0.1 nanosecond wide pedestal pulse. Note that the HEMPV result has been scaled down by a factor of four.

Fig. 6. EMP computed by MACSYNC for 1 kt total yield with a 0.3% gamma fraction, 3 Mev gamma energy, and a 0.1 nanosecond wide pedestal pulse.

Fig. 7. Linear amplitude plot of the two thick curves shown in Fig. 6. The contributions to the total field from sources radiating either inside or outside the shadow cone region are shown separately.

Fig. 8. The total field for three different yields, either without a gamma shield or with a shield having a $1e-4$ transmission factor. The gamma fraction is 0.3%, the gamma energy is 3 Mev, and the pulse is a 0.1 nanosecond wide pedestal.